StarD13 differentially regulates migration and invasion in Prostate cancer cells

Leila Jaafar[1], Isabelle Fakhoury[1], Sahar Saab[1], Wassim Abou-Kheir[2] and Mirvat El-Sibai[1]*

[1]*Department of Natural Sciences, School of Arts and Sciences, Lebanese American University, Beirut, Lebanon*

[2]*Department of Anatomy, Cell Biology and Physiological Sciences, Faculty of Medicine, American University of Beirut, Beirut, Lebanon*

*Corresponding author:
Mirvat El-Sibai, PhD
Associate Professor
Department of Natural Sciences
Lebanese American University
P.O. Box: 13-5053
Chouran 1102 2801, Beirut, Lebanon
Email: mirvat.elsibai@lau.edu.lb
Phone: +961-1-786456, Ext 1709
Fax: +961-1-867098

Abstract

Prostate cancer is the second most commonly diagnosed cancer in men and one of the main leading causes of cancer deaths among men worldwide. Rapid uncontrolled growth and the ability to metastasize to other sites are key hallmarks in cancer development and progression. The Rho family of GTPases and its activators the GTPase-activating proteins (GAPs) are required for regulating cancer cell proliferation and migration. StarD13 is a GAP for Rho GTPases, specifically for RhoA and Cdc42. We have previously shown that StarD13 acts as a tumor suppressor in astrocytoma as well as breast and colorectal cancer. In this study, we performed a functional comparative analysis of StarD13 targets/and or interacting molecules to understand the general role that StarD13 plays in cancers. We then investigated the role of StarD13 in prostate cancer, specifically with regards to cell proliferation and metastasis. Our data highlight the importance of StarD13 in modulating several hallmarks of cancer. Findings from database mining and immunohistochemistry further revealed that StarD13 is underexpressed in prostate cancers consistent with its role as a tumor suppressor. Knocking down StarD13 using siRNA also showed that inhibiting StarD13 increases cancer cell proliferation in 2D and thus confirming its role as a tumor suppressor. Interestingly, we noted that StarD13 depletion increases invasion and matrix degradation of prostate cancer cells but suppresses cell migration in 2D through enhanced adhesion. Altogether, the data presented suggests that StarD13 acts as a tumor suppressor which is also required for promoting prostate cancer cell motility in 2D.

Keywords: StarD13, Rho GAP, Rho GTPases, Prostate cancer, Metastasis, Cell motility

Introduction

Most prostate cancers are adenocarcinomas which occur in the prostate gland present exclusively in males. They are the second most common type of cancer that affects men in the US. In 2020, the American Cancer Society estimated that there will be around 191,930 new cases of prostate cancer and 33,330 deaths among men from prostate cancer (1).

Tumor invasion and metastasis remain the major causes of deaths in prostate cancer patients (2, 3). Cancer metastasis is the migration of cancer cells from the primary tumor site to a distant location in the body. This process starts with tumor cells downregulating adhesion proteins and detaching from the primary tumor and is followed by degradation and invasion of the underlying extracellular matrix until reaching the blood or a lymphatic vessel (2-4). Cell motility regulation is a core process in metastasis. It involves the transduction of a series of pathways which lead to the actin cytoskeleton remodeling at the leading edge of the cell and the formation of cytoplasmic protrusions called lamellipodia and filopodia (5). Then the actin polymers are stabilized by adhering to the substrate through the focal adhesions at the front end of the cell, while the rear end retracts by detaching the focal adhesions from the extracellular matrix (ECM) (6-8).

The Rho family of GTPases is the main regulator of actin cytoskeleton dynamics and cell motility (9, 10). Rho GTPases alternate between an active GTP-bound form and an inactive GDP-bound form. The Rho family of GTPases and its activators the GTPase-activating proteins (GAPs) have been linked to various cellular processes which are deregulated in cancer including cell cycle progression, vesicular trafficking, cell polarity, and cell motility (11). StarD13 also called DLC2,

is a Rho GAP for Rho GTPases, specifically for Rho A and Cdc42 (12). GAPs enhance the intrinsic GTPase activity of Rho GTPases which leads to the hydrolysis of the GTP and therefore, their inactivation (13, 14). StarD13 plays a tumor suppressor role in many cancers (15, 16). It is often found deleted in cancer tissues but the expression of StarD13 has also been predictive of an overall good prognosis (17).

Mechanistically, StarD13 has been shown to inhibit Ras signaling and Ras-induced cellular transformation (15). It also suppressed cell growth by inhibiting the Raf-1-ERK1/2-p70S6K signaling pathway (15, 18). Moreover, StarD13 regulated pro-apoptotic factors such as caspase-3, Bax, and BMF (19). Finally, StarD13 regulated cell motility, EMT transition and the metastasis of different tumors (20-26).

Little is known about the role of StarD13 in prostate cancer. Therefore, in this study we assessed the overall expression of StarD13 in normal and prostate cancer tissue, and determined the role of StarD13 in prostate cancer proliferation, 2D migration and 3D motility.

Materials and Methods

Antibodies and Reagents

Rabbit polyclonal anti-StarD13 antibody, mouse monoclonal anti-actin antibody, and rabbit polyclonal anti-Tks4 antibody were purchased from Abcam (Abcam Inc., Cambridge, UK) Mouse monoclonal anti-StarD13 antibody and rabbit monoclonal anti-paxillin antibody were obtained from Santa Cruz Biotechnology (Santa-Cruz Inc., California, USA). Anti-rabbit and anti-mouse HRP-conjugated secondary antibodies were ordered from Promega (Promega Co., Wisconsin, USA). Fluorescent secondary goat anti-rabbit and goat anti-mouse antibodies (Alexa Fluor 488-green) as well as Rhodamine phalloidin were purchased from Invitrogen (Invitrogen, Massachussets, USA). DAPI stain was obtained from Roche Diagnostics (Roche Ltd, Mannheim, Germany). Hiperfect transfection reagent, luciferase GL2 and human Flexi Tubes siRNA for StarD13 (oligos 3 and 8) were bought from Qiagen (Qiagen N.V., Hilden, Germany).

Cell Culture

PC3 and DU145 prostate cancer cell lines were purchased from ATCC (American Type Culture Collection). The cells were cultured in RPMI-1640 AQ media supplemented with 10% fetal bovine serum, 1% non-essential amino acids, and 100U penicillin/streptomycin and kept in a humidified chamber at 37°C and 5% CO_2.

Bioinformatic analysis

STARD13 targets identified by literature review were classified according to their biological processes, molecular functions and genes ontology pathways using the PANTHER bioinformatics software (Protein ANalysis Through Evolutionary Relationships). Subsequently, the targets

networks and interactions map was constructed in STRING database (Search Tool for the Retrieval of Interacting Genes/Proteins). Specifically, we set the minimum required interaction score to high confidence (0.7) and limited the active interaction sources to information fished from textmining, experimentally determined interactions, and curated databases. We then eliminated the non-connected nodes and generated the cluster map.

mRNA Expression Analysis

To determine the expression of StarD13 in human prostate tumors, we mined the publicly available Repository Oncoming gene expression microarray database (National Cancer Institute, https://www.oncomine.org/resource/login.html). Data was plotted using the normal versus prostate cancer data sets and parameters and the threshold was set at p-value of 0.001.

Immunohistochemistry

Paraffin-embedded tissue slides of normal and adenosis of prostate tissues were purchased from OriGene technologies (OriGene Technologies Inc, Maryland, USA). The slides were deparaffinized by soaking in xylol before hydration by consecutive washes in ethanol. After removing the paraffin by rinsing under tap water, the tissues were re-hydrated by soaking in PBS for 20 minutes at room temperature. Next, 200-300ml of antigen retrieval buffer (1mM EDTA pH=8) were heated in a 700W microwave for 5 min and added to the slides which were also microwaved twice for 5 min with a 1 min break in between. Following, the tissues were surrounded with a water repellent material (clear nail polish), blocked in a 4% blocking solution (PBS+4% BSA+0.1% Triton-X 100) at room temperature and then incubated with mouse monoclonal anti-StarD13 antibody (1:300) for 2 hours. Afterwards, the slides were washed with ice-cold PBS. And

incubated with a secondary anti-mouse antibody coupled to Alexa fluor-488 fluorophore for 30 min at room temperature. Finally, the slides were washed and mounted using a mounting solution from mixed with DAPI. Fluorescent images were taken on a Zeiss Observer Z1 microscope (20X) (Zeiss, Oberkochen, Germany).

Cell Transfection with siRNA

DU145 cells were transfected with predesigned siRNA directed against human StarD13 at a final concentration of 10 nM using Hiperfect according to the manufacturer's recommendations. Control cells were transfected with siRNA sequences targeting GL2 Luciferase. Western blot analysis was performed 72 hours post-transfection to determine the expression level of StarD13 protein. Alternatively, the effect of the knock down was also assessed at 72 hours post-transfection using the appropriate antibodies; or the effect of the corresponding knockdown was assessed.

Western Blot

Whole-cell lysates were obtained after scraping the cells with laemmli sample buffer containing 4% SDS, 20% glycerol, 10% β-mercaptoethanol, 0.004% bromophenol blue, and 0.125M Tris HCL (pH 6.8). SDS-PAGE was then carried out under standard conditions and proteins were blotted onto a PVDF membrane as previously described (22, 24, 27-29). Following, the membranes were blocked with 5% bovine serum albumin for 1 hour and incubated overnight at 4°C with either primary antibody against StarD13 (1:200) or actin (1:2500). After incubation with the primary antibody, the membranes were washed and incubated with the appropriate secondary antibody (1:1000) for 1 hour at room temperature. Finally, the membranes were washed, and the bands were visualized using a chemiluminescent reagent ECL (GE Healthcare). Protein expression

levels were measured by densitometry analysis in the ImageJ software (National Institutes of Health, Massachusetts, USA).

Sphere Formation Assay

DU145 cell suspension was chilled on ice, before mixing 2000 cells/condition with thawed Matrigel from Corning (Corning Inc, New York, USA) in a 1:1 ratio. Next, 100 µl of the master mix were plated over the well rims of a 24 well-plate and incubated at 37 °C for 45-60 min to allow matrigel solidification before adding 700 µl of 5% FBS RPMI-1640 AQ media and transfection with siRNA. The cells were then incubated with 100 µl of a transfection master mix and either Luciferase, StarD13 oligo 3, or StarD13 oligo 8 siRNA for 72 hours. Finally, the media and the transfection mix were replenished every 3 days for a total of 13 days and cell images were snapped using a light microscope (10x) and quantified in the ZEN software.

Sphere Immunostaining

The spheres were collected and fixed with 4% PFA then permeabilized using 0.5% Triton X. After blocking in the blocking solution (0.1% BSA, 0.2% Triton X-1000, and 0.05% Tween-20) for 2 hours, the spheres were incubated with the primary anti-StarD13 over-night at 4 °C. The next day, the spheres were washed with a PBST (PBS containing 0.1% Tween-20) then incubated with the Alexa-488 conjugated secondary antibody for 2 hours. Finally, the spheres were washed and pelleted before mixing with 5-7µl of anti-fade reagent mixed with DAPI.. The mounted slides were sealed and imaged using the 20x objective lens on the Zeiss Observer Z1 microscope.

Cell proliferation Assay

DU145 prostate cancer cells were seeded in a 96-well plate and transfected with siRNA targeting either Luciferase or StarD13. Cell viability was determined by adding 20µl of the WST-1 reagent to the wells and incubating the cells for 2 hours in a humidified incubator at 37 ℃ and 5% CO_2. The color change caused by the cleavage of the tetrazolium salt into formazan was quantified at 450nm using an ELISA plate reader.

Motility Assay (Time-Lapse)

For cell motility analysis, transfected DU145 cells were imaged randomly moving in RPMI-1640 AQ (10% FBS, 1% non-essential amino acid) media at 37 °C 5% CO_2. Cell images were collected every 60 seconds for 2 hours using a 20X objective lens on the Zeiss Observer Z1 microscope. The total distance traveled by DU145 cells was quantified using the ROI tracker plugin in the ImageJ software. The speed (µm/min) of at least 10 individual cells per condition was then calculated by dividing the total distance traveled over time.

Wound Healing Assay

DU145 cells were grown to confluence before making a wound with a sterile pipette tip. Next, the plates were washed to remove cell debris and fresh medium was replenished. Phase-contrast images of the wound area were taken at T=0 and 24 hours later using the 10X objective of a Leica inverted microscope. Wound widths were measured at 11 different positions for each condition, and the average rate of wound closure was calculated in µm/hr using the ImageJ software.

Adhesion Assay

Cell adhesion assay was performed as previously described (27). Briefly, 96-well plates were coated with collagen type I overnight at 37°C. After washing with washing buffer (0.1% BSA in RPMI-1620 AQ media), the plates were blocked with 0.5% BSA in RPMI-1620 AQ media at 37°C in a CO_2 incubator for 1 hour. DU145 cells were trypsinized and diluted to the density of $4x10^5$cell/ml. 50 µl of the cell suspension was added to each well and the plate was incubated at 37°C in a 5% CO_2 incubator for 30 minutes. Next, the plates were shaken and the wells were washed 3 times before fixation in 4% paraformaldehyde at room temperature for 10 minutes. Washed cells were then stained with crystal violet (5 mg/ml in 2% ethanol) for 10 minutes. Finally, the plates were washed extensively with water and left to dry completely before solubilizing crystal violet in 2% SDS for 30 minutes and quantification of the absorption at 550 nm using an ELISA plate reader.

Immunocytochemistry

Cells plated on glass coverslips were treated as indicated, before fixation in 4% paraformaldehyde for 10 minutes at 37°C. Next, DU145 cells were permeabilized with 0.5% Triton-X for 15 minutes on ice, and incubated with 0.1 M glycine for 10 minutes. The coverslips were then blocked, 1% filtered BSA solution before incubation with the primary antibodies overnight at 4°C and with fluorophore-conjugated secondary antibodies for 1 hour the following day. Fluorescent images were taken using a 63x objective lens on the Zeiss Observer Z1 microscope.

Gelatin Invadopodia Assay

The invasion ability of DU145 cells was measured using the QCM Gelatin Invadopodia Assay (Green) kit from Millipore (Millipore, Massachusetts, USA). Briefly, the cells were plated on fluorescently labeled gelatin matrix and incubated at 37 °C and 5% CO_2 for 24 hours before staining with Tks-4.Fluorescent images were taken using a 63X objective lens on Zeiss Observer Z1 microscope operated by the Zen software (Zeiss, Oberkochen, Germany).. The area devoid of fluorescence and intensity of the Tks-4 signal was analyzed using ImageJ software.

For invadopodia assays, the cells were transfected then plated on Alexa 568-conjugated matrix-coated glass coverslips (30) (QCM Gelatin Invadopodia Assay-Millipore, MA, USA) for 48 hours to measure the total degradation. For individual invadopodia detection, the cells were plated on Alexa 568-conjugated matrix for 8 hours only. Next, the cells were fixed with 4% paraformaldehyde for 10 minutes at 37ºC and permeabilized with 0.5% Triton-X 100 for 15 minutes on ice. Following, the samples cells were blocked in 1% BSA solution for 1 hour, before incubation with primary antibodies overnight at 4ºC, and with fluorophore-conjugated secondary antibodies for 1 hour. Fluorescent images were taken using a 63X objective lens on Zeiss Observer Z1 microscope operated by the Zen software (Zeiss, Oberkochen, Germany).

Quantification of Spheres

The ZEN Image Analysis software was used to quantify at least 50 spheres per condition. All images were set to scale before determining the diameter of each sphere using the circle tool.

Quantification of Focal Adhesions

ImageJ CLAHE and Log3D plugins used for local contrast enhancement and image filtering,

respectively, were applied to vinculin stained cell images. This allowed the detection and quantification of focal adhesions. The data was presented as the size area fold difference relative to the control.

Statistical Analysis

The results were obtained from at least three independent experiments. The data is presented as the mean ± SEM. The p-values were calculated using t-test and statistical significance was set at p-value ≤ 0.05.

Results

StarD13 Regulates Cancer-Related Hallmarks and Pathways

To understand the role of STARD13 in tumors, we searched the literature for molecules which interact with STARD13 or which can be regulated by STARD13 in different cancers (Table 1). We then performed a functional comparative analysis of the listed STARD13 targets/interacting partners using the Protein ANalysis THrough Evolutionary Relationships (PANTHER) database. Specifically, we classified the genes according to their molecular functions (Figure 1A), the biological processes they regulate (Figure 1B), as well as the pathways in which they have been reported (Figure 1C). As expected, the targets possessed specific molecular functions which conferred the ability to regulate key biological processes that are of vital importance to cancer onset and progression. The results showed that StarD13 targets have catalytic (cyclins, TAZ, ROCK, ERK, Cdc42, Rac1, FKBP51, RhoA,), binding (RhoA, Rac1, Cdc42, HOXB4, ROCK, CDH5, CTGF, cyclins, Bax), and regulatory (TAZ, Sox2, HOXB4, cyclins, paxillin) functions (Figure 1A). Moreover, these proteins are involved in proliferation, biogenesis, development (ErbB2, RhoA, ERK, ROCK, Rac1, cyclins, paxillin, Sox2, HOXB4, CDH5, TP53INP1, etc.), adhesion (CTGF, paxillin, CDH5), and cell motility (Cdc42, paxillin, ERK, Rac1, RhoA) processes (Figure 1B). In addition, the targets ontology pathways highlight the importance of STARD13 in cancer because of its ability to modulate several hallmarks of cancer, namely, cell death and apoptosis (p53, bax, bcl-2, Fas), cell cycle and proliferation (ErbB2, p38, ERK, cyclins), angiogenesis, inflammation as well as cell motility by regulation of the cytoskeleton by the Rho GTPases pathway (Rac, cdc42, RhoA, ROCK, paxillin, cadherins, integrin) (Figure 1C). Finally,

we searched for possible protein-protein interactions between STARD13 and its targets and constructed the pathway using STRING database. The global interaction proteome network of is presented in Figure 1D. Specifically, the map indicates the presence of interactions between STARD13 and RhoA which is in line with the GAP function of STARD13. Using this approach, we found that proteins belonging to different structural and functional families involved in processes such as angiogenesis, stemness, apoptosis and proliferation are enriched. This further shows that the Rho GTPase pathway remains at the center of this map, with STARD13 connecting to the PI3K and MAPK pathways through Rac1.

StarD13 is Under Expressed in Prostate Cancer

After having determined the importance of StarD13 in cancer regulation and the potential mechanisms implicated in StarD13 mediated signaling, we sought to explore the role of StarD13 in prostate cancer. First, we mined the oncomine database for microarray analysis of available StarD13 mRNA expression levels from normal and prostate adenocarcinoma tissues. The datasets obtained in Figure 2A show that StarD13 is underexpressed in tumor tissues as compared to normal ones. (grade 0). This was further confirmed by immunohistochemistry StarD13 signal intensity was 16% lower in prostate cancer tissues when compared to the normal ones (Figures 2B and 2C).

StarD13 is a Tumor Suppressor in Prostate Cancer Cells Grown in 2D

To further understand the role of StarD13 in prostate cancer, StarD13 was knocked down in two different cell lines: DU145 (Figure 3A) and PC3 (Figure 3B) cancer cells. This was done by transfecting the cells with StarD13 specific si-RNA (oligo 1 and oligo 2), or a nonspecific negative control (Luciferase siRNA). Western blot analysis showed that both oligos used were efficient in

inhibiting the expression of StarD13. Specifically, StarD13 expression levels were reduced by 5 folds in DU145 cells as compared to the control (Luciferase siRNA) in DU145 cells (Figure 3A). Similarly, StarD13 expression levels were reduced by 3.5 (oligo 1) to 2 folds (oligo 2) in PC3 cells as compared to the control (Figure 3B).

After having proved the knock down efficiency of the oligos used, we measured the proliferative activity of Du145 cells and PC3 depleted of StarD13 using the WST-1 assay. Figure 3C shows that StarD13 depletion leads to a 32% (oligo 1) and 22% (oligo 2) increase in DU145 cell proliferation, respectively when compared to the control (Luciferase siRNA). Similarly, a significant increase in the proliferation of PC3 cells was observed upon StarD13 knock down (Figure 3C).

StarD13 is a Tumor Suppressor in Prostate Cancer Cells Grown in 3D

To mimic tissue-like behavior, we grew DU145 and PC3 spheres using the sphere formation assay and studied StarD13 functions in 3D. Both sphere models were transfected with StarD13 siRNA oligo 1, 2 or a non-specific control (Luciferase siRNA) as described previously. The efficiency of StarD13 depletion however was tested by immunostaining the DU145 spheres (Figure 4A) or PC3 spheres (Figure 4C) with anti StarD13 and determining the intensity of the fluorescent signal. Figure 4A shows a 65.4% and 68.8% reduction in StarD13 signal in Du145 spheres transfected with StarD13 siRNA oligo 1 and 2, respectively as compared to the control. StarD13 signal was also significantly reduced in PC3 spheres transfected with StarD13 siRNA oligo 1 and 2, respectively as compared to the control (Figure 4C). Next, we investigated the effect of StarD13 depletion on the area of DU145 and PC3 spheres as well as the rate of sphere formation which are

both reflective of the proliferative activity of the cells in 3D (Figure 4B and 4D). The area of single spheres and the rate of sphere formation were measured 12 days after the transfection with the corresponding siRNA. Depletion of StarD13 using StarD13 siRNA oligo 1 and 2 increased DU145 sphere area by 66% and 38%, respectively as compared to the control (Figure 4B). As expected the sphere forming unit also significantly increased in response to StarD13 depletion (Figure 4B). Similarly, StarD13 depletion using StarD13 siRNA oligo 1 and 2 significantly increased PC3 sphere area and the sphere forming unit, as compared to the control (Figure 4D). Finally, we were able to show that the proliferation of DU145 spheres is inversely proportional to StarD13 expression (Figure 4E).

StarD13 Promotes Prostate Cancer Cell Motility in 2D by Enhancing Adhesion

After having established the anti-proliferative potential of StarD13 in 2D and 3D models of prostate cancer, we tested the molecule's ability to modulate cell motility using two approaches: wound healing, and time-lapse assay. Knocking down StarD13 in DU145 cells by transfecting decreased the rate of wound closure by 45% (oligo 1) and 51% (oligo 2), respectively as compared to the control (Figure 5A). The time lapse assay also demonstrated that knocking down StarD13 reduces the net movement and speed of the cells. Specifically, silencing StarD13 led to a 43% and 53.8% decrease in net distance migrated by Du145 cells that were transfected by StarD13 siRNA oligo 1 and 1, respectively (Figure 5B and supplemental movies S1 and S2).

To understand the mechanism by which StarD13 depletion inhibits cell motility in 2D, and in light of StarD13 potential regulation of cellular adhesion processes determined earlier on (Figure 1B), we assessed StarD13 knock down effects on the adhesion of DU145 cells to collagen, a major component of the ECM. Figure 5C reveals 35% and 65% increase in cellular adhesion of DU145

cells transfected with StarD13 siRNA oligo 1 and 2, respectively as compared to the control. Immunoblotting for focal adhesions which are actin-rich structures used by the cell to adhere to the underlying matrix, further supported this finding. Indeed, DU145 cells were stained with anti-paxillin antibody after knocking down StarD13 (Figure 5D). Paxillin is a marker of focal adhesions and was also identified as a target of StarD13 (Table1). Our data shows that the depletion of StarD13 increases the area of focal adhesions by 9% (oligo 1) and 8.2% (oligo 2), respectively as compared to control. Moreover, the silencing of StarD13 triggered 70% (oligo 1) and 120% (oligo 2) increase in the number of focal adhesions respectively when compared to Luciferase (Figure 5D).

StarD13 Depletion Increases Invasion and Matrix Degradation of Prostate Cancer Cells

Matrix degradation is a critical step in cancer invasion and metastasis. MMP2 and MMP9 metalloproteinases proteins are required for extracellular matrix degradation therefore we investigated the effects of knocking down StarD13 on the expression levels of these proteins (Figures 6A and 6B). Both proteins expressions levels were increased when StarD13 was depleted. Specifically, StarD13 knock down led to a 3.5 to 4.5 fold increase in MMP2 expression (Figure 6A) and a 2 to 3 fold increase in MMP9 expression levels (Figure 6B).

Using a transwell migration assay and FBS as a chemoattractant in the lower wells, we depleted StarD13 in DU145 cells before assessing their ability to invade *in* vitro in a collagen-based invasion assay. Compared to the control, DU145 cells depleted of StarD13 exhibited a 2.5 fold increase in invasion as compared to the control (Figure 6C). An increase in invasion of StarD13-depleted cells was already suspected due to the invasive phenotype of the stard13-depleted spheres

(Figure 4B, 4D and 4E), compared to the smooth encapsulated edge of the controls. This was further supported by the gelatin invadopodia assay findings. Briefly, StarD13 was silenced before plating DU145 cells on fluorescently labeled gelatin (matrix) and incubating at 37 °C and 5% CO_2 for 24 hours. After staining with Tks-4, a marker of invadopodia and one of the main factors needed for invadopodia assembly (31), we show that StarD13 depletion by StarD13 siRNA oligo 1 and 2 increase the invaded area by 14% (oligo 1) and 20% (oligo2), respectively (Figure 6D). Moreover, the intensity of the Tks-4 signal increases by 15% and 13.4% in DU145 cells upon knocking down StarD13 using oligos 1 and 2 respectively (Figure 6D).

Discussion

We performed this study to understand the role of StarD13 in prostate cancer. We began by predicting the pathways and biological processes that StarD13 is most likely to affect. Using bioinformatics tools we showed that StarD13 targets genes with functions that are critical for cell proliferation and cell motility including binding, catalysis, regulation, signal transduction, epigenetic modulation, and molecular export functions. This is in line with previous studies which have reported StarD13 ability to modulate different cancer hallmarks including proliferation, cell motility and invasion (12, 23, 25, 32). Moreover, this is consistent with StarD13 function as a RhoGAP for Rho GTPases which are known for their roles in regulating cell proliferation, biogenesis, adhesion, apoptosis, angiogenesis, inflammation, and cell motility among other (9, 10, 14, 33-36).

To study StarD13 in prostate cancer, we first quantified its expression levels in normal and low-grade prostate cancer tissues. Data from the different datasets examined in oncomine as well as immunohistochemistry results confirmed that StarD13 is underexpressed in prostate cancer. This is in agreement with the literature, whereby StarD13 expression is often reduced in various cancer tissues due to gene deletions, epigenetics regulation, or copy loss (16, 20, 22, 37-41). High expression levels of StarD13 on the other hand, have been associated with better prognosis for patients with cancer (17, 41). Altogether, this suggests a tumor suppressor function for StarD13 in prostate cancer similar to that we and others have observed in breast cancer, astrocytoma, colorectal cancer, and hepatocellular carcinoma (16, 21, 22, 42).

We proved that StarD13 plays a tumor suppressor role in prostate cancer cells in 2D and 3D after depleting the cells of this protein and assessing the effects on cell proliferation. StarD13 depletion increased cell viability of prostate cancer cells in 2D, and the sphere area and rate of sphere formation of the prostate cancer spheres grown in 3D.

Tumor invasion and metastasis remain the major causes of deaths in patients with prostate cancer. Our functional analysis also highlighted a potential role for StarD13 in modulating cell motility and invasion. Indeed, using both wound assay and random motility assays we demonstrated that the depletion of StarD13 decreases cell motility of prostate cancer cells in 2D. Promoting cell motility is an unconventional behavior for a tumor suppressor. However, this corroborates with our previous results which uncovered a cell motility promoting function for StarD13 in breast cancer, astrocytoma, and colorectal cancer (16, 22, 24)

The first step in cancer invasion and metastasis is the downregulation of adhesion. This allows the cells to detach from the tumor and move into the neighboring tissues (43-48). Hence, it was critical to test the effect of StarD13 on cell adhesion and invasion to understand the mechanism by which StarD13 regulates 3D cell motility. Knocking down StarD13 increased prostate cancer cells ability to adhere to collagen as well as increased the number and area of focal adhesions as demonstrated by paxillin staining. Interestingly, we had identified paxillin as a target for StarD13 and these experiments further proved the regulation of paxillin by starD13 in prostate cancer. However, cell motility and cell adhesion findings were contradictory. Cellular motility depends on cycles of cell adhesion and detachment from the ECM. However, the data suggested that more adhesion and less cell motility were taking place simultaneously in response to StarD13 depletion.

One possible explanation can be attributed to the Rho GAP nature of StarD13. Specifically, StarD13 is a Rho GAP to Rho A which is in turn responsible for focal adhesion formation. Hence, the depletion of StarD13 can potentially trigger a constitutive activation of Rho A, thus enhancing cell adhesion to the substrate while reducing cell motility. We have indeed demonstrated that the regulation of Rho A at the focal adhesions by StarD13 is important for astrocytoma cell motility (49). A similar mechanism might be taking place in the prostate cancer cell lines used in this study. Alternatively, cell motility consists of cycles of attachment to the ECM at the front end of the cell and detachment at the rear end. Therefore examining the localization of StarD13 in a motile cell can be a potential mean to explaining this behavior.

Testing StarD13 effects on prostate cancer cell invasion we showed that StarD13 depletion increases the expression levels of the metalloproteases proteins MMP-2 and MMP-9. Cancer cells express and secrete MMP enzymes through their invadopodia structures to degrade the extracellular matrix and invade into the surrounding tissues (4). Consistent with the increase in MMP expression, depletion of StarD13 increased prostate cancer cell invasion as evidenced by the transwell assay and gelatin invadopodia assay. The expression of the Tks-4 marker of invadopodia was also increased in response to StarD13 further confirming the importance of StarD13 in inhibiting cell invasion. To our knowledge, this was the first report of MMP and TKs-4 regulation by StarD13. More importantly, both the upregulation of MMPs expression levels and invadopodia formation upon StarD13 highlight the negative role that StarD13 plays in prostate cancer 3D cell motility (invasion). This finding is in agreement with the tumor suppressor role played by StarD13 in prostate cancer however, it contradicts StarD13 effects on 2D cell motility in the same tumor. Nevertheless, this behavior is consistent with previous studies carried out in our laboratory that

evaluated the StarD13 effects on cell invasion in different tumor types (16, 22, 24). Future studies, are still warranted to assess the role of Star13 in prostate cancer onset, notably with regards to the processes related to stemness that we have identified by gene ontology. Finally, it is imperative to elaborate on the crosstalk between the family of Rho GTPases and StarD13 in the formation of invadopodia and focal adhesions in prostate cancer cells.

Conclusion

In this study we showed that StarD13 is involved in many aspects of cancer malignancy including cell proliferation, biogenesis, angiogenesis, and cell motility. We also demonstrated that StarD13 is underexpressed in prostate cancer tumors and acts as a tumor suppressor in 2D and 3D cultures. Interestingly, we established that StarD13 is a positive regulator of 2D cell motility but not 3D. Mechanistically, we proved that StarD13 stimulation of cell motility in 2D involves the downregulation of focal adhesion formation. Altogether, the data highlights the role of StarD13 in suppressing the main hallmarks of cancer, namely, cell proliferation, adhesion, and invasion. In parallel, we uncovered a positive contribution of StarD13 to the 2D cellular motility of prostate cancer cells. In conclusion, StarD13 ability to modulate different aspects of cancer malignancy such as proliferation, motility, and invasion makes it a great candidate for cancer therapeutics.

Acknowledgment

The ROI Tracker was supplied by David Entenberg and John Condeelis as supported by CA100324 and GM064346. This work was funded by the Department of Natural Sciences at the Lebanese

American University and by the School of Arts and Science Research and Development Council (SRDC) at LAU.

Conflict of interest

The authors declare that they have no conflict of interest.

Author contributions

Leila Jaafar performed experiments and data analysis

Isabelle Fakhoury performed experiments and data analysis and wrote the manuscript

Sahar Saab performed experiments

Wassim Abou-Kheir provided intellectual and technical guidance

Mirvat El-Sibai is the principal investigator who designed the study, provided funds, critical data analysis and discussion and edited the manuscript

Figure Legends

Table 1. StarD13 directly and indirectly targets and/or interacts with a wide number of molecules in different tumor types.

Figure 1. Gene ontology and network pathway analysis highlight StarD13 central role in cell signaling, motility and cancer modulation. **A.** Pie chart representing the molecular functions of StarD13 targets. **B.** Pie chart representing the biological processes of StarD13 targets. **C.** Pie chart representing StarD13 target genes ontology pathways. **D.** Pathways and Networks Modulated by StarD13 and its Targets. Global pathway analysis of the 36 potential targets of StarD13 was performed using STRING database. The network nodes are proteins whose final position in the network is computed by minimization of the energy of the system. The color of the lines refers to the source predicting the active interaction. Green: texmining, pink: experimentally determined, and blue: curated databases.

Figure 2. StarD13 is Under Expressed in Prostate Cancer. A. Data analyzed from Oncomine website data sets. StarD13 mRNA samples were quantified and the results were plotted using the normal versus prostate cancer data sets. **B.** Immunohistochemistry of normal prostate tissue (top micrograph) and adenosis of prostate tissue (lower micrograph) against StarD13 (green), DAPI (blue), and a merge image between StarD13 and DAPI. Tissues were visualized on a 20x lens of a fluorescent microscope. **C.** Quantification of StarD13 expression using ImageJ software. Data are the mean -/+ SEM from 3 assays. The results were significant with $p<0.05$.

Figure 3. StarD13 is a tumor suppressor in prostate cancer cells. Prostate cancer cells were transfected with Luciferase siRNA, StarD13 siRNA oligo 1, or oligo 2 for 72 hours. Cells were lysed and blotted against StarD13. **A.** Left panel: Western blot profile showing the expression levels of StarD13 and actin in DU145 cancer cells. Right panel: Quantification of StarD13 expression by ImageJ software. **B.** Left panel: Western blot profile showing the expression of StarD13 and actin in PC3 cancer cells. Right panel: Quantification of StarD13 expression by ImageJ software. **C.** Cell viability of Luciferase siRNA and StarD13 siRNA (oligo 1 and oligo 2) transfected DU145 cells (left panel) and PC3 cells (right panel) was expressed as fold increase relative to the control (right panel). Data are the mean -/+ SEM from 3 assays. The results were significant with $p<0.05$.

Figure 4. StarD13 suppresses prostate cancer cell proliferation in 3D spheres. DU145 and PC3 cells were transfected with Luciferase siRNA, StarD13 siRNA oligo 1, or oligo 2, and images were taken 12 days after transfection. **A.** Left panel: Micrographs illustrating DU145 spheres transfected with Luciferase siRNA or StarD13 siRNA oligo 1, or oligo 2 and stained for StarD13 (green). Right panel: Quantitation of knock down efficiency of StarD13 expressed as % StarD13 fluorescent intensity normalized to the control Luciferase siRNA. **B.** Left panel: Sphere micrographs illustrating the morphology of DU145 spheres transfected with Luciferase siRNA or StarD13 siRNA oligo 1 or oligo 2. Right panel: Quantitation of spheres sphere forming unit of DU145 cells transfected with Luciferase siRNA, StarD13 siRNA oligo 1 or oligo 2. The Data are the mean -/+ SEM from three different trials. The results were significant with $p<0.05$. **C.** Left panel: Micrographs illustrating PC3 spheres transfected with Luciferase siRNA or StarD13 siRNA oligo 1, or oligo 2 and stained for StarD13 (green). Right panel: Quantitation of knock down efficiency of StarD13 expressed as % StarD13 fluorescent intensity normalized to the control Luciferase siRNA. **D.** Left panel: Sphere micrographs illustrating the morphology of PC3 spheres transfected with Luciferase siRNA or StarD13 siRNA oligo 1 or oligo 2. Right panel: Quantitation of spheres sphere forming unit of PC33 cells transfected with Luciferase siRNA, StarD13 siRNA oligo 1 or oligo 2. The Data are the mean -/+ SEM from three different trials. The results were significant with $p<0.05$. **E.** DU145 spheres were formed from DU145 cells transfected with

Luciferase siRNA, or StarD13 siRNA and stained for StarD13 (green), rhodamine phalloidin (orange) and DAPI (blue). Left panel: Micrographs showing DU145 spheres in response to decreasing StarD13 expression levels. Right panel: Quantification of DU145 spheres area in response to decreasing StarD13 intensity. Data are the mean -/+ SEM from 3 assays. The results were significant with $p<0.05$.

Figure 5. StarD13 depletion suppresses cell migration through enhanced adhesion. A. DU145 cells were transfected with Luciferase siRNA, or StarD13 siRNA for 72 hours. A wound was created, and images were taken in the same frame at t=0 and after 24 hours. Left panel: Wound profile at t=0 and t=24hrs. Right panel: Quantification of wound closure rate in fold changes as compared to Luciferase siRNA. Data are the mean -/+ SEM from 3 assays. The results were significant with $p<0.05$. Scale bar is 100 µm **B.** DU145 cells were transfected with Luciferase siRNA, StarD13 siRNA oligo 1, or oligo 2 for 72 hours and imaged moving in media randomly. The average migrated distance (in µm) was quantitated using ImageJ software and the speed (in µm/min) was obtained by dividing the distance over 120 minutes. ***C.*** Left panel: Representative images of cells that were fixed and stained with crystal violet to detect adhesion of Luciferase siRNA or StarD13 siRNA transfected DU145 cells. Scale bar is 100 µm. Right panel: Quantitation of stained cells by colorimetric measurement using ELISA (560 nm). Data are the mean -/+ SEM from 2 assays. The results were significant with $p<0.05$. **D.** Left panel: Representative micrographs of DU145 cells transfected with si-luciferase or si-StarD13 and immunostained with paxillin (green) and Rhodamine phalloidin (orange). Cells were imaged using a 63x objective. Right panel: Quantification of the area of focal adhesions and number of focal adhesions.

Figure 6. StarD13 depletion increases invasion and matrix degradation of prostate cancer cells. A. Left panel: Western blot profile showing the expression levels of MMP-2 and actin in DU145 cancer cells transfected with Luciferase siRNA or StarD13 siRNA. Right panel: Quantification of MMP-2 expression by ImageJ software. **B.** Left panel: Western blot profile showing the expression levels of MMP-9 and actin in DU145 cancer cells transfected with Luciferase siRNA or StarD13 siRNA. Right panel: Quantification of MMP-9 expression by ImageJ software. **C.** Left panel: Representative micrographs of DU145 transfected with Luciferase siRNA or StarD13 siRNA at the bottom of collagen-coated membranes. The cells were allowed to invade towards 10% FBS for 24 h. Scale bar is 100 µm. Right panel: Quantification of the invaded cells after cell stain extraction. Data were measured in arbitrary units. **D.** DU145 cells were transfected with Luciferase siRNA, or StarD13 siRNA and plated on fluorescently labeled gelatin, then the cells were stained against Tks-4 to mark invadopodia. Left panel: Micrographs showing the change in invaded area (orange), intensity of Tks-4 (green), and DAPI (blue). Images were visualized using a 64x lens of a fluorescent microscope and quantified using ImageJ software. Scale bar is 20 µm. Right panel: Quantification of area invaded by DU145 cells as well as the intensity of Tks-4.

Supplementary Material

Supplemental movie S1. Time-lapse movie of DU145 control cells undergoing random motility
Supplemental movie S2. Time-lapse movie of DU145 cells with StarD13 knock down undergoing random motility.

References

1. Key statistics for prostate cancer | prostate cancer facts: American Cancer Society; [updated January 8, 2020. Available from: https://www.cancer.org/cancer/prostate-cancer/about/key-statistics.html.

2. Christofori G. New signals from the invasive front. Nature. 2006;441(7092):444-50.
3. Gupta GP, Massagué J. Cancer metastasis: building a framework. Cell. 2006;127(4):679-95.
4. Zeeshan R, Mutahir Z. Cancer metastasis - tricks of the trade. Bosn J Basic Med Sci. 2017;17(3):172-82.
5. Alblazi KM, Siar CH. Cellular protrusions--lamellipodia, filopodia, invadopodia and podosomes--and their roles in progression of orofacial tumours: current understanding. Asian Pacific journal of cancer prevention : APJCP. 2015;16(6):2187-91.
6. Bailly M, Condeelis J. Cell motility: insights from the backstage. Nature cell biology. 2002;4(12):E292-4.
7. Lauffenburger DA, Horwitz AF. Cell migration: a physically integrated molecular process. Cell. 1996;84(3):359-69.
8. Michaelis UR. Mechanisms of endothelial cell migration. Cellular and molecular life sciences : CMLS. 2014;71(21):4131-48.
9. Hanna S, El-Sibai M. Signaling networks of Rho GTPases in cell motility. Cellular signalling. 2013;25(10):1955-61.
10. Al-Koussa H, Atat OE, Jaafar L, Tashjian H, El-Sibai M. The Role of Rho GTPases in Motility and Invasion of Glioblastoma Cells. Anal Cell Pathol (Amst). 2020;2020:9274016.
11. Heasman SJ, Ridley AJ. Mammalian Rho GTPases: new insights into their functions from in vivo studies. Nat Rev Mol Cell Biol. 2008;9(9):690-701.
12. Ching YP, Wong CM, Chan SF, Leung TH, Ng DC, Jin DY, et al. Deleted in liver cancer (DLC) 2 encodes a RhoGAP protein with growth suppressor function and is underexpressed in hepatocellular carcinoma. The Journal of biological chemistry. 2003;278(12):10824-30.
13. Ridley AJ. Rho GTPase signalling in cell migration. Curr Opin Cell Biol. 2015;36:103-12.
14. Alan JK, Lundquist EA. Mutationally activated Rho GTPases in cancer. Small GTPases. 2013;4(3):159-63.
15. El-Sitt S, El-Sibai M. The STAR of the DLC family. J Recept Signal Transduct Res. 2013;33(1):10-3.
16. El-Sitt S, Khalil BD, Hanna S, El-Sabban M, Fakhreddine N, El-Sibai M. DLC2/StarD13 plays a role of a tumor suppressor in astrocytoma. Oncology reports. 2012;28(2):511-8.
17. Gao F, Yu X, Meng R, Wang J, Jia L. STARD13 is positively correlated with good prognosis and enhances 5-FU sensitivity via suppressing cancer stemness in hepatocellular carcinoma cells. Onco Targets Ther. 2018;11:5371-81.
18. Leung TH, Yam JW, Chan LK, Ching YP, Ng IO. Deleted in liver cancer 2 suppresses cell growth via the regulation of the Raf-1-ERK1/2-p70S6K signalling pathway. Liver Int. 2010;30(9):1315-23.
19. Guo X, Xiang C, Zhang Z, Zhang F, Xi T, Zheng L. Displacement of Bax by BMF Mediates STARD13 3'UTR-Induced Breast Cancer Cells Apoptosis in an miRNA-Depedent Manner. Mol Pharm. 2018;15(1):63-71.
20. Ullmannova V, Popescu NC. Expression profile of the tumor suppressor genes DLC-1 and DLC-2 in solid tumors. International journal of oncology. 2006;29(5):1127-32.
21. Basak P, Leslie H, Dillon RL, Muller WJ, Raouf A, Mowat MRA. In vivo evidence supporting a metastasis suppressor role for Stard13 (Dlc2) in ErbB2 (Neu) oncogene induced mouse mammary tumors. Genes Chromosomes Cancer. 2018;57(4):182-91.

22. Hanna S, Khalil B, Nasrallah A, Saykali BA, Sobh R, Nasser S, et al. StarD13 is a tumor suppressor in breast cancer that regulates cell motility and invasion. International journal of oncology. 2014;44(5):1499-511.
23. Li X, Zheng L, Zhang F, Hu J, Chou J, Liu Y, et al. STARD13-correlated ceRNA network inhibits EMT and metastasis of breast cancer. Oncotarget. 2016;7(17):23197-211.
24. Nasrallah A, Saykali B, Al Dimassi S, Khoury N, Hanna S, El-Sibai M. Effect of StarD13 on colorectal cancer proliferation, motility and invasion. Oncology reports. 2014;31(1):505-15.
25. Yang B, Zhou SN, Tan JN, Huang J, Chen ZT, Zhong GY, et al. Long Non-Coding RNA STARD13-AS Suppresses Cell Proliferation And Metastasis In Colorectal Cancer. Onco Targets Ther. 2019;12:9309-18.
26. Zhou G, Liu X, Xiong B, Sun Y. Homeobox B4 inhibits breast cancer cell migration by directly binding to StAR-related lipid transfer domain protein 13. Oncology letters. 2017;14(4):4625-32.
27. Al Hassan M, Fakhoury I, El Masri Z, Ghazale N, Dennaoui R, El Atat O, et al. Metformin Treatment Inhibits Motility and Invasion of Glioblastoma Cancer Cells. Anal Cell Pathol (Amst). 2018;2018:5917470.
28. Al-Dimassi S, Salloum G, Saykali B, Khoury O, Liu S, Leppla SH, et al. Targeting the MAP kinase pathway in astrocytoma cells using a recombinant anthrax lethal toxin as a way to inhibit cell motility and invasion. International journal of oncology. 2016;48(5):1913-20.
29. Nicolas S, Abdellatef S, Haddad MA, Fakhoury I, El-Sibai M. Hypoxia and EGF Stimulation Regulate VEGF Expression in Human Glioblastoma Multiforme (GBM) Cells by Differential Regulation of the PI3K/Rho-GTPase and MAPK Pathways. Cells. 2019;8(11).
30. Yamaguchi H, Lorenz M, Kempiak S, Sarmiento C, Coniglio S, Symons M, et al. Molecular mechanisms of invadopodium formation: the role of the N-WASP-Arp2/3 complex pathway and cofilin. J Cell Biol. 2005;168(3):441-52.
31. Iizuka S, Abdullah C, Buschman MD, Diaz B, Courtneidge SA. The role of Tks adaptor proteins in invadopodia formation, growth and metastasis of melanoma. Oncotarget. 2016;7(48):78473-86.
32. Zheng L, Li X, Chou J, Xiang C, Guo Q, Zhang Z, et al. StarD13 3'-untranslated region functions as a ceRNA for TP53INP1 in prohibiting migration and invasion of breast cancer cells by regulating miR-125b activity. European journal of cell biology. 2018;97(1):23-31.
33. Bishop AL, Hall A. Rho GTPases and their effector proteins. Biochem J. 2000;348 Pt 2(Pt 2):241-55.
34. Boettner B, Van Aelst L. The role of Rho GTPases in disease development. Gene. 2002;286(2):155-74.
35. Jaffe AB, Hall A. Rho GTPases: biochemistry and biology. Annual review of cell and developmental biology. 2005;21:247-69.
36. Parsons JT, Horwitz AR, Schwartz MA. Cell adhesion: integrating cytoskeletal dynamics and cellular tension. Nat Rev Mol Cell Biol. 2010;11(9):633-43.
37. Hankins GR, Sasaki T, Lieu AS, Saulle D, Karimi K, Li JZ, et al. Identification of the deleted in liver cancer 1 gene, DLC1, as a candidate meningioma tumor suppressor. Neurosurgery. 2008;63(4):771-80; discussion 80-1.
38. de Tayrac M, Etcheverry A, Aubry M, Saïkali S, Hamlat A, Quillien V, et al. Integrative genome-wide analysis reveals a robust genomic glioblastoma signature associated with copy number driving changes in gene expression. Genes Chromosomes Cancer. 2009;48(1):55-68.

39. Wang D, Qian X, Rajaram M, Durkin ME, Lowy DR. DLC1 is the principal biologically-relevant down-regulated DLC family member in several cancers. Oncotarget. 2016;7(29):45144-57.
40. Wolosz D, Walczak A, Szparecki G, Dwojak M, Winiarska M, Wolinska E, et al. Deleted in Liver Cancer 2 (DLC2) protein expression in hepatocellular carcinoma. Eur J Histochem. 2019;63(1).
41. Sun L, Sun J, Song JD. High expression of DLC family proteins predicts better prognosis and inhibits tumor progression in NSCLC. Molecular medicine reports. 2019;19(6):4881-9.
42. Zhang H, Wang F, Hu Y. STARD13 promotes hepatocellular carcinoma apoptosis by acting as a ceRNA for Fas. Biotechnol Lett. 2017;39(2):207-17.
43. Lu Z, Jiang G, Blume-Jensen P, Hunter T. Epidermal growth factor-induced tumor cell invasion and metastasis initiated by dephosphorylation and downregulation of focal adhesion kinase. Mol Cell Biol. 2001;21(12):4016-31.
44. Okabe H, Aoki K, Yogosawa S, Saito M, Marumo K, Yoshida K. Downregulation of CD24 suppresses bone metastasis of lung cancer. Cancer Sci. 2018;109(1):112-20.
45. Tang H, Jiang L, Zhu C, Liu R, Wu Y, Yan Q, et al. Loss of cell adhesion molecule L1 like promotes tumor growth and metastasis in esophageal squamous cell carcinoma. Oncogene. 2019;38(17):3119-33.
46. Saykali BA, El-Sibai M. Invadopodia, regulation, and assembly in cancer cell invasion. Cell communication & adhesion. 2014;21(4):207-12.
47. Steeg PS. Targeting metastasis. Nature reviews Cancer. 2016;16(4):201-18.
48. Gardel ML, Schneider IC, Aratyn-Schaus Y, Waterman CM. Mechanical integration of actin and adhesion dynamics in cell migration. Annual review of cell and developmental biology. 2010;26:315-33.
49. Khalil BD, Hanna S, Saykali BA, El-Sitt S, Nasrallah A, Marston D, et al. The regulation of RhoA at focal adhesions by StarD13 is important for astrocytoma cell motility. Experimental cell research. 2014;321(2):109-22.

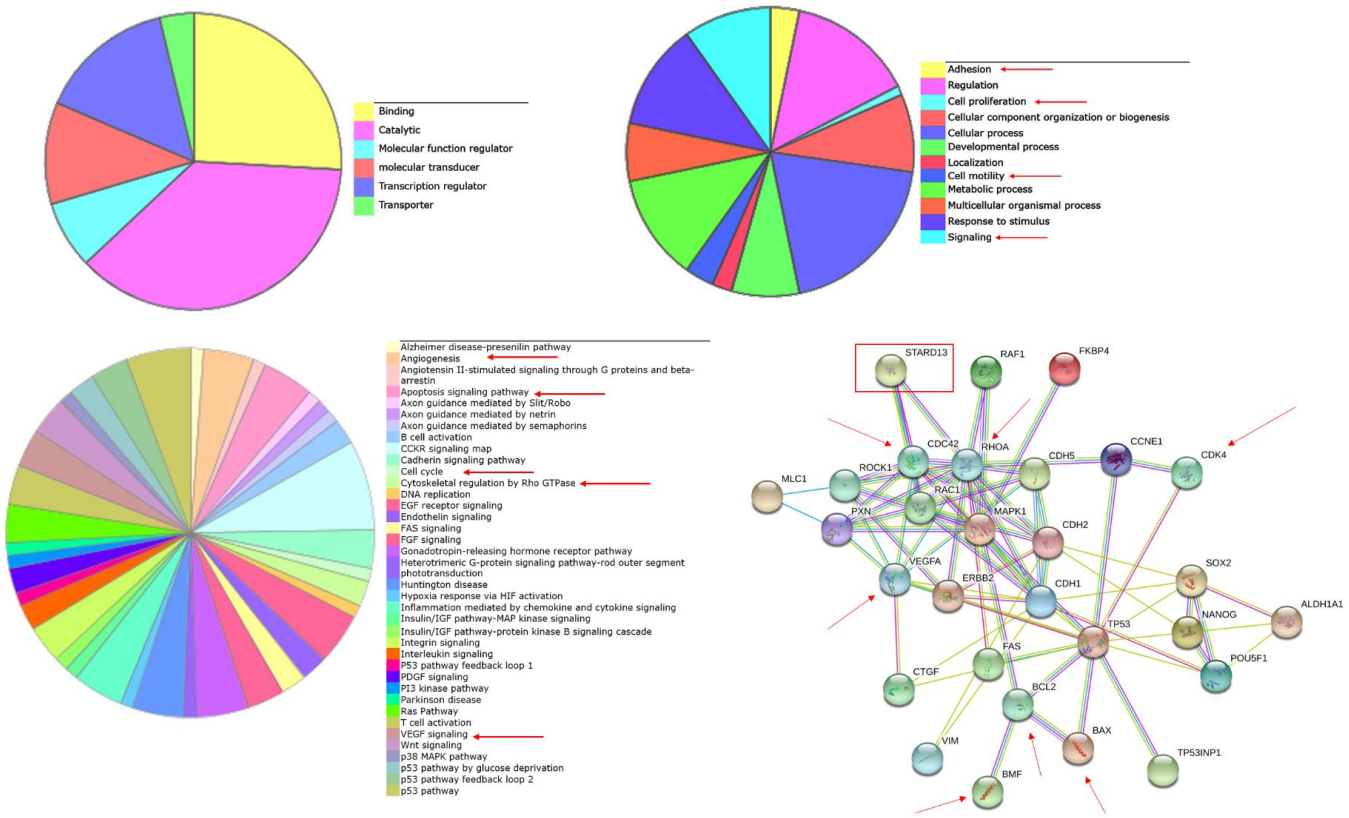
Binding
Catalytic
Molecular function regulator
molecular transducer
Transcription regulator
Transporter
Adhesion
Regulation
Cell proliferation
Cellular component organization or biogenesis
Cellular process
Developmental process
Localization
Cell motility
Metabolic process
Multicellular organismal process
Response to stimulus
Signaling
Alzheimer disease-presenilin pathway
Angiogenesis
Angiotensin II-stimulated signaling through G proteins and beta-arrestin
Apoptosis signaling pathway
Axon guidance mediated by Slit/Robo
Axon guidance mediated by netrin
Axon guidance mediated by semaphorins
B cell activation
CCKR signaling map
Cadherin signaling pathway
Cell cycle
Cytoskeletal regulation by Rho GTPase
DNA replication
EGF receptor signaling
Endothelin signaling
FAS signaling
FGF signaling
Gonadotropin-releasing hormone receptor pathway
Heterotrimeric G-protein signaling pathway-rod outer segment phototransduction
Huntington disease
Hypoxia response via HIF activation
Inflammation mediated by chemokine and cytokine signaling
Insulin/IGF pathway-MAP kinase signaling
Insulin/IGF pathway-protein kinase B signaling cascade
Integrin signaling
Interleukin signaling
P53 pathway feedback loop 1
PDGF signaling
PI3 kinase pathway
Parkinson disease
Ras Pathway
T cell activation
VEGF signaling
Wnt signaling
p38 MAPK pathway
p53 pathway by glucose deprivation
p53 pathway feedback loop 2
p53 pathway
STARD13
RAF1
FKBP4
CDC42
RHOA
CDH5
CCNE1
CDK4
ROCK1
MLC1
RAC1
PXN
MAPK1
CDH2
VEGFA
ERBB2
CDH1
SOX2
ALDH1A1
NANOG
TP53
FAS
POU5F1
CTGF
BCL2
BAX
VIM
TP53INP1
BMF

Figure1

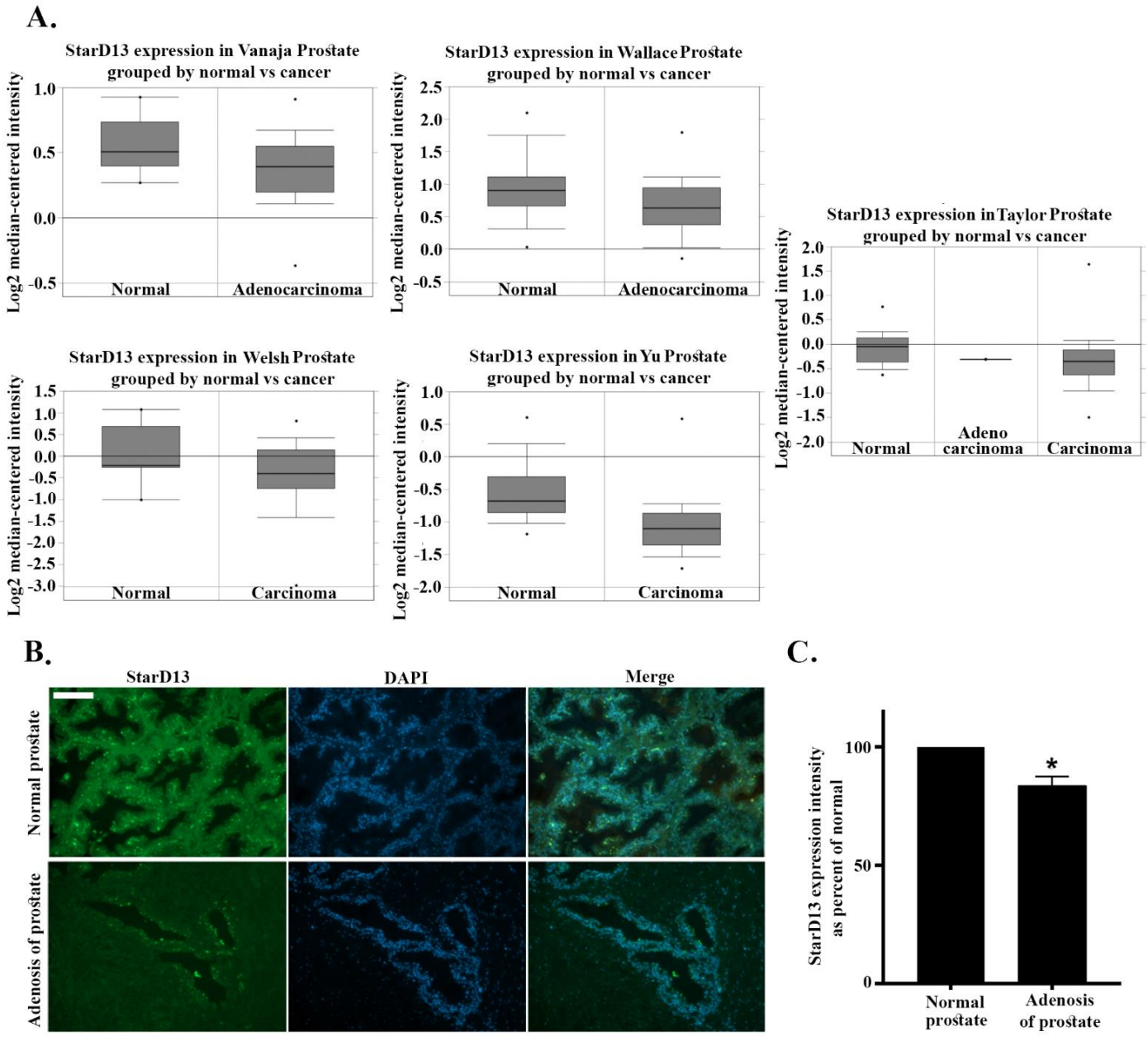
A.
StarD13 expression in Vanaja Prostate grouped by normal vs cancer
Log2 median-centered intensity
Normal
Adenocarcinoma
StarD13 expression in Wallace Prostate grouped by normal vs cancer
Log2 median-centered intensity
Normal
Adenocarcinoma
StarD13 expression in Taylor Prostate grouped by normal vs cancer
Log2 median-centered intensity
Normal
Adeno carcinoma
Carcinoma
StarD13 expression in Welsh Prostate grouped by normal vs cancer
Log2 median-centered intensity
Normal
Carcinoma
StarD13 expression in Yu Prostate grouped by normal vs cancer
Log2 median-centered intensity
Normal
Carcinoma
B.
StarD13
DAPI
Merge
Normal prostate
Adenosis of prostate
C.
StarD13 expression intensity as percent of normal
100
50
0
*
Normal prostate
Adenosis of prostate

Figure2

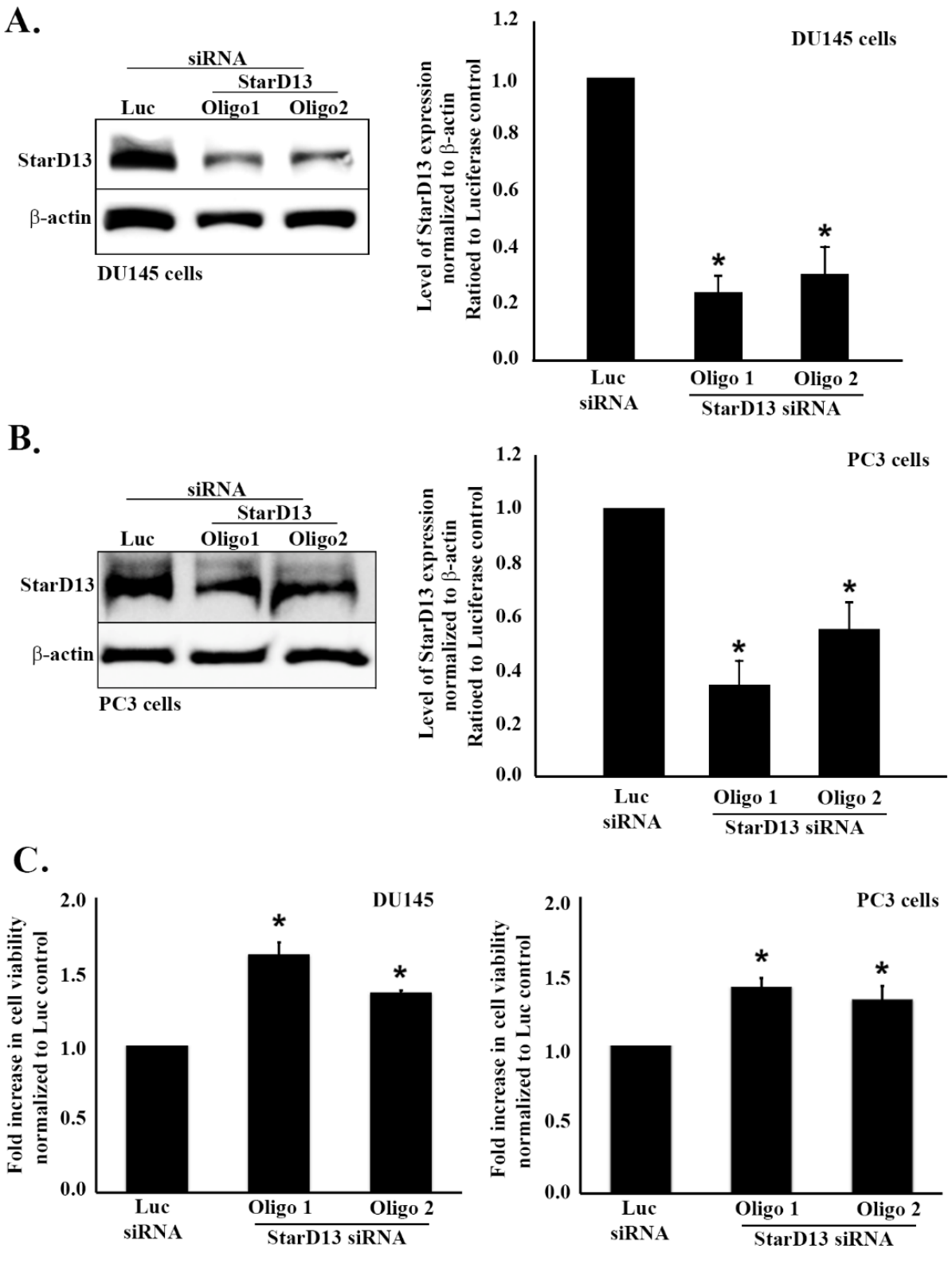
A.
siRNA
StarD13
Luc
Oligo1
Oligo2
StarD13
β-actin
DU145 cells
Level of StarD13 expression normalized to β-actin Ratioed to Luciferase control
DU145 cells
1.2
1.0
0.8
0.6
0.4
0.2
0.0
Luc siRNA
Oligo 1
Oligo 2
StarD13 siRNA
B.
siRNA
StarD13
Luc
Oligo1
Oligo2
StarD13
β-actin
PC3 cells
Level of StarD13 expression normalized to β-actin Ratioed to Luciferase control
PC3 cells
1.2
1.0
0.8
0.6
0.4
0.2
0.0
Luc siRNA
Oligo 1
Oligo 2
StarD13 siRNA
C.
Fold increase in cell viability normalized to Luc control
DU145
2.0
1.5
1.0
0.5
0.0
Luc siRNA
Oligo 1
Oligo 2
StarD13 siRNA
Fold increase in cell viability normalized to Luc control
PC3 cells
2.0
1.5
1.0
0.5
0.0
Luc siRNA
Oligo 1
Oligo 2
StarD13 siRNA

Figure3

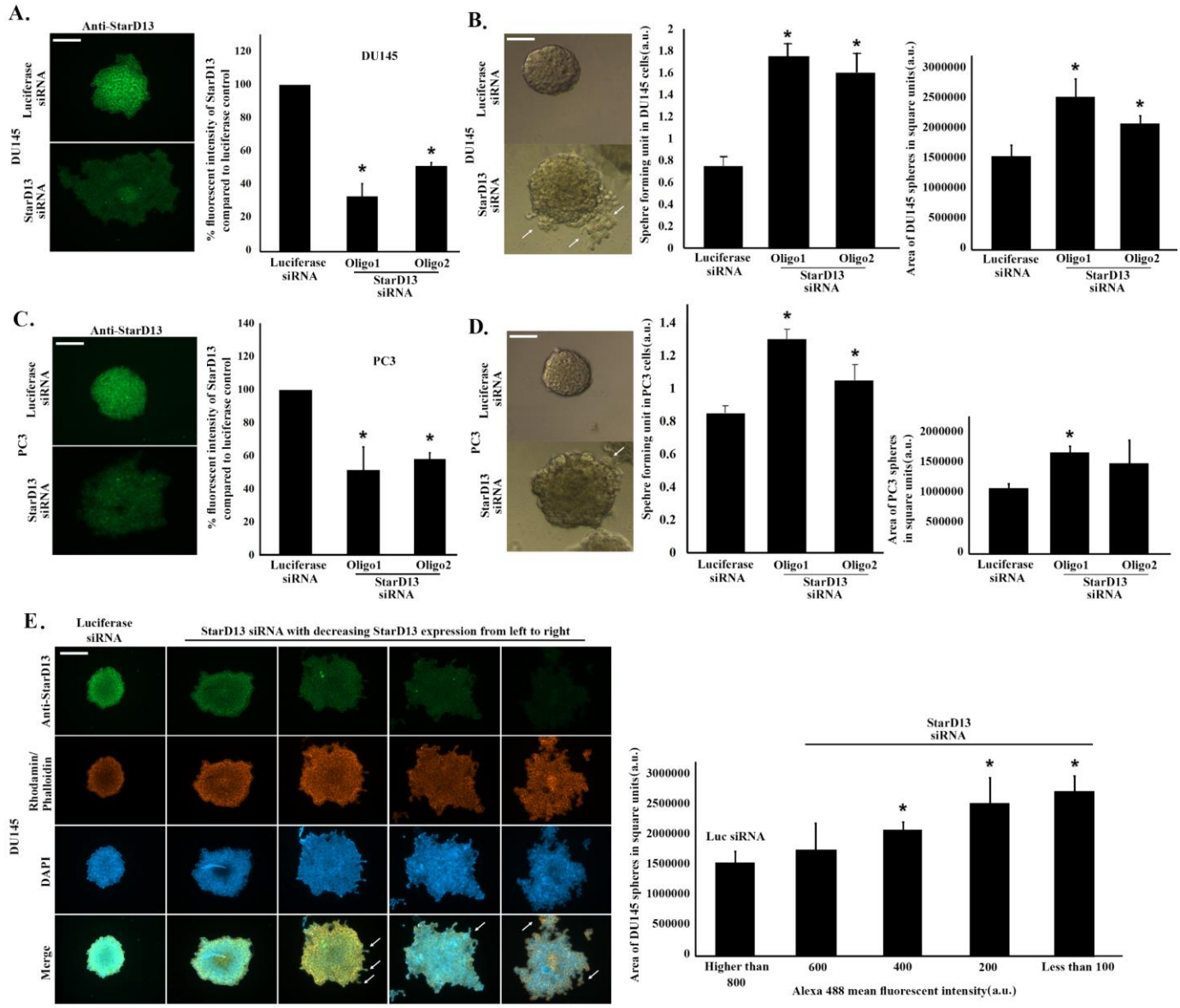
A.
Anti-StarD13
DU145
Luciferase siRNA
StarD13 siRNA
% fluorescent intensity of StarD13 compared to luciferase control
DU145
Luciferase siRNA
Oligo1
Oligo2
StarD13 siRNA
B.
Sphere forming unit in DU145 cells(a.u.)
Area of DU145 spheres in square units(a.u.)
C.
Anti-StarD13
PC3
% fluorescent intensity of StarD13 compared to luciferase control
PC3
D.
Sphere forming unit in PC3 cells(a.u.)
Area of PC3 spheres in square units(a.u.)
E.
Luciferase siRNA
StarD13 siRNA with decreasing StarD13 expression from left to right
Anti-StarD13
Rhodamin/ Phalloidin
DAPI
Merge
DU145
StarD13 siRNA
Luc siRNA
Area of DU145 spheres in square units(a.u.)
Higher than 800
600
400
200
Less than 100
Alexa 488 mean fluorescent intensity(a.u.)

Figure4

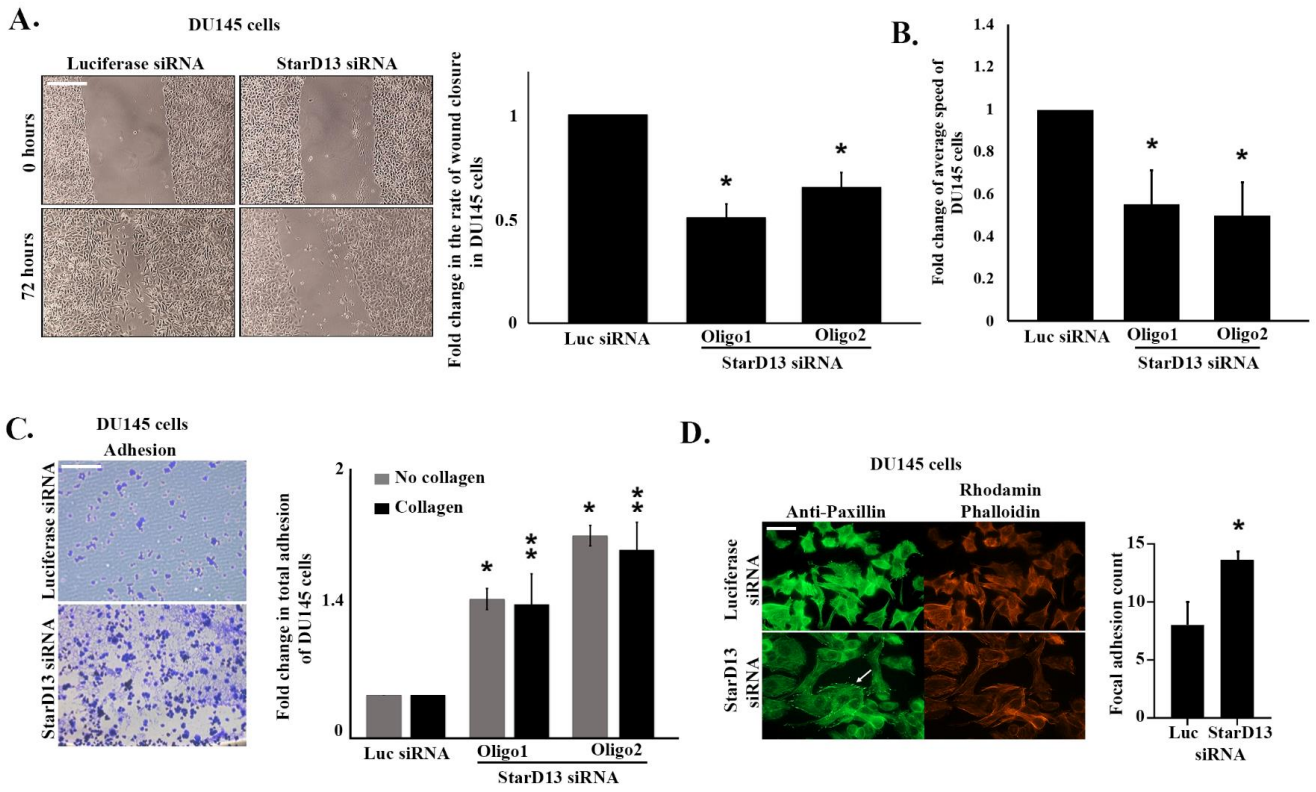

Figure5

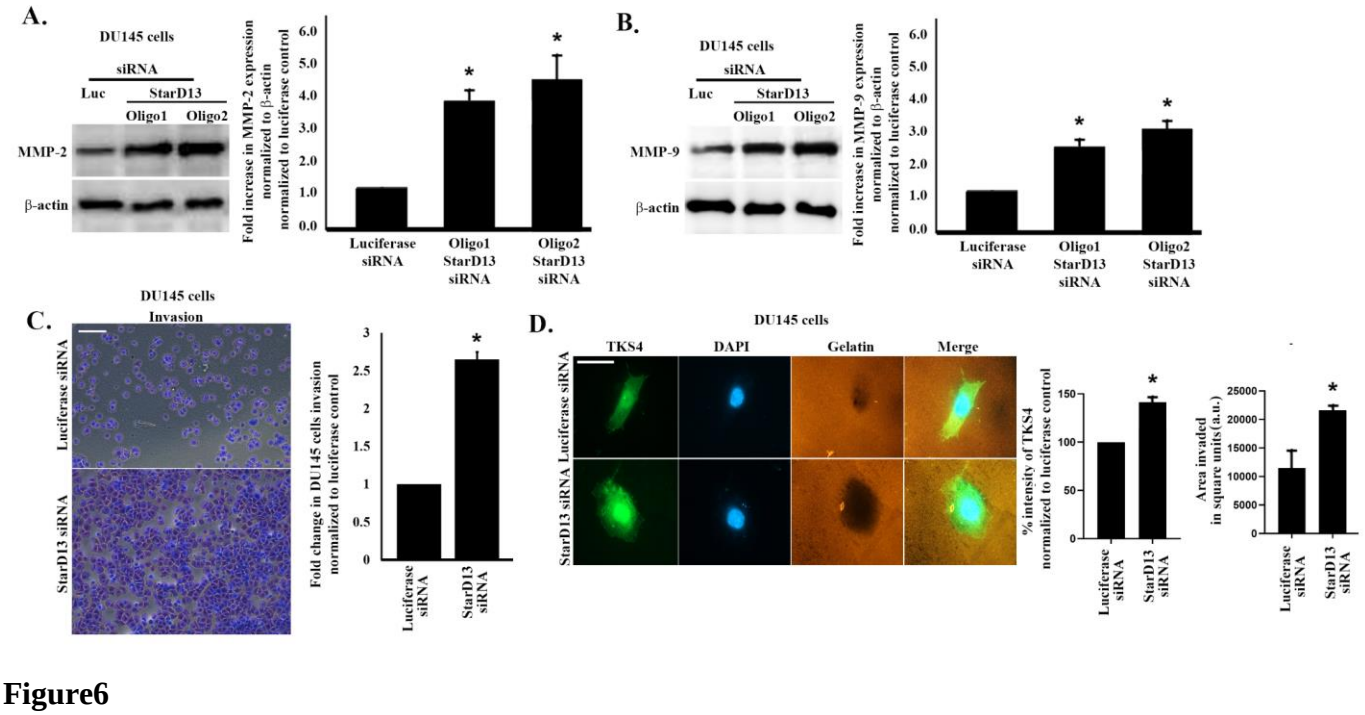

Figure6

Cancer Type	STARD13 Modulated/Interacting Targets				
Brain	Cdc42, pERK, Rac, Rho A (El-Sitt et al., 2012; Khalil et al., 2014; Nicolas, Abdellatef, Haddad, Fakhoury, & El-Sibai, 2019)	VEGF-A (Nicolas, Abdellatef, Haddad, Fakhoury, & El-Sibai, 2019)			
	Rho A, Rac (Hanna et al., 2014)	ErbB2 (Basak et al., 2018)	CDH5, HOXD1, HOXD10, Integrin, Vimentin, E-Cadherin (Zheng, Xiang et al., 2018)	RNPC1, CDH5, HOXD10, HOXD1 (Zheng, Zhang et al., 2018)	TP53INP1 (Zheng, Li et al., 2018)
Breast	YAP, TAZ, Rho A, Rock, MLC, ALDH1, OCT3/4, Sox2, Nanog, CTGF, CDH5, HOXD1, HOXD10 (Zheng et al., 2018)	HOXB4, Rho A (Zhou, Liu, Xiong, & Sun, 2017)	BMF, Bax, Bcl-2 (Guo et al., 2018)	FKBP51 (Takaoka, Ito, Miki, & Nakanishi, 2017)	
Bone	PUM2 (Hu et al., 2018)				
Colon	p53, Bcl-2, Bax, Cdc42, Rac, Rho A (Nasrallah et al., 2014)	Cyclin D, Cyclin E, E-Cadherin, N-Cadherin, Vimentin (Yang et al., 2019)			
Liver	Fas (Zhang, Wang, & Hu, 2017)	Raf-1, ERK1/2, p70S6K, Paxillin (Leung, Yam, Chan, Ching, & Ng, 2010)	Rho A, pMLC-S19, YAP, CTGF, ALDH1, Nanog (Gao, Yu, Meng, Wang, & Jia, 2018)		
Prostate	E-cadherin N-cadherin Vimentin (Chen et al., 2019)				

Table1